2018

Distributions of total and size-fractionated particulate 210Po and 210Pb activities along the North Atlantic GEOTRACES GA01 transect: GEOVIDE cruise

Yi Tang

Maxi Castrillejo

Montserrat Roca-Marti

Pere Masque´
Edith Cowan University, p.masque@ecu.edu.au

Nolwenn Lemaitre

See next page for additional authors

10.5194/bg-15-5437-2018
Tang, Y., Castrillejo, M., Roca-Martí, M., Masqué, P., Lemaitre, N., & Stewart, G. (2018). Distributions of total and size-fractionated particulate 210 Po and 210 Pb activities along the North Atlantic GEOTRACES GA01 transect: GEOVIDE cruise. *Biogeosciences*, *15*(17), 5437-5453. Available here

Biogeosciences, 15, 5437–5453, 2018
https://doi.org/10.5194/bg-15-5437-2018

Biogeosciences Open Access EGU

Distributions of total and size-fractionated particulate ^{210}Po and ^{210}Pb activities along the North Atlantic GEOTRACES GA01 transect: GEOVIDE cruise

Yi Tang[1,2], **Maxi Castrillejo**[3,4], **Montserrat Roca-Martí**[3], **Pere Masqué**[3,5], **Nolwenn Lemaitre**[6], **and Gillian Stewart**[2,1]

[1]Earth and Environmental Sciences, the Graduate Center, City University of New York, New York, USA
[2]School of Earth and Environmental Sciences, Queens College, City University of New York, Flushing, USA
[3]Institut de Ciència i Tecnologia Ambientals & Departament de Física, Universitat Autònoma de Barcelona, Bellaterra, 08193, Spain
[4]Laboratory of Ion Beam Physics, ETH Zurich, Otto-Stern-Weg 5, Zürich, 8093, Switzerland
[5]School of Science and Centre for Marine Ecosystems Research, Edith Cowan University, Joondalup, Western Australia, Australia
[6]Department of Earth Sciences, Institute of Geochemistry and Petrology, ETH Zurich, Zürich, Switzerland

Correspondence: Gillian Stewart (gillian.stewart@qc.cuny.edu)

Received: 30 April 2018 – Discussion started: 15 May 2018
Revised: 19 August 2018 – Accepted: 24 August 2018 – Published: 14 September 2018

Abstract. Vertical distributions of total and particulate polonium-210 (^{210}Po) and lead-210 (^{210}Pb) activities in the water column were measured at 11 stations in the North Atlantic during the GEOTRACES GA01 transect: GEOVIDE cruise in May–June 2014. Total ^{210}Po activity was on average 24 % lower than ^{210}Pb activity in the upper 100 m, and it was closer to unity in the mesopelagic (100–1000 m). The partitioning coefficients (K_d) along the transect suggest the preferential association of ^{210}Po relative to ^{210}Pb onto particles. The prominent role of small particles in sorption was confirmed by the observation that over 80 % of the particulate radionuclide activity was on small particles. To account for the observed surface water ^{210}Po / ^{210}Pb disequilibria, particulate radionuclide activities and export of both small (1–53 µm) and large (> 53 µm) particles must be considered. A comparison between the GEOVIDE total particulate ^{210}Po / ^{210}Pb activity ratios (ARs) and the ratios in previous studies revealed a distinct geographic distribution, with lower particulate ARs in the high-latitude North Atlantic (including this study) and Arctic in relation to all other samples. For the samples where apparent oxygen utilization (AOU) was calculated at the same depth and time as the ^{210}Po / ^{210}Pb AR (40 stations including this study), there was a two-phase correlation between the total particulate AR and AOU, likely reflecting the nature of the particles and demonstrating the forces of remineralization and radionuclide decay from particles as they age.

1 Introduction

The major goal of the international GEOTRACES program is to characterize the distributions of trace elements and isotopes (TEIs) in the ocean on a global scale, and to identify and quantify processes that control these distributions (GEOTRACES Planning Group, 2006). The GEOVIDE section was a contribution of the French GEOTRACES program to this global program in the subpolar North Atlantic. The GEOVIDE GA01 cruise was carried out in 2014 in the North Atlantic and consisted of two sections: a section along the OVIDE (Observatoire de la variabilité interannuelle et décennale en Atlantique Nord) line between Lisbon (Portugal) and Cape Farewell (southern tip of Greenland), and a Cape Farewell–St. John's (Canada) section across the Labrador Sea (Fig. 1). Since 2002, the OVIDE section has been occupied biennially to collect physical and biogeochemical data (Mercier et al., 2015). The knowledge of the currents, water masses, and biogeochemical provinces gained from the

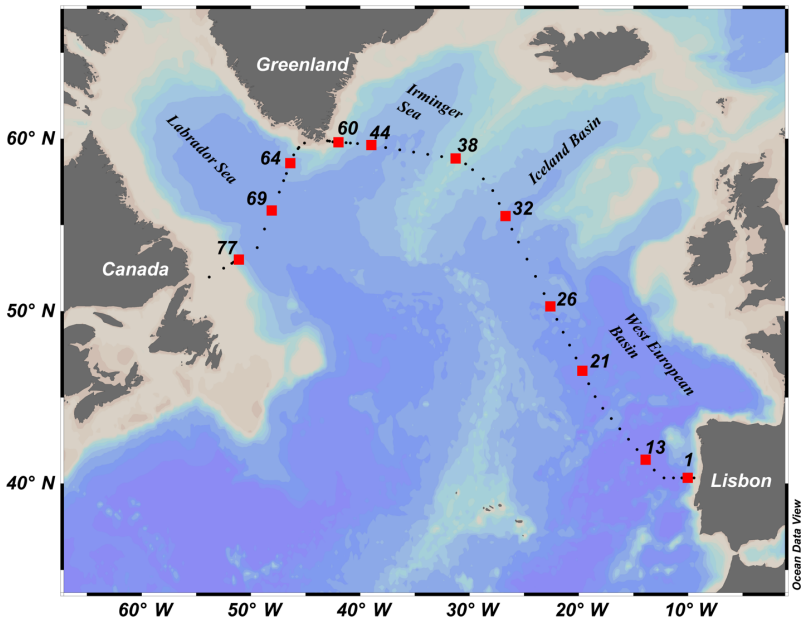

Figure 1. Map of the GEOVIDE cruise track (black dots) and the 11 stations sampled for ^{210}Po and ^{210}Pb activity (red squares). Each sampling location is labeled with a station number. The sampling stations are divided into four regions (from east to west): West European Basin (stations 1, 13, 21, 26), Iceland Basin (stations 32, 38), Irminger Sea (stations 44, 60), and Labrador Sea (stations 64, 69, 77).

previous OVIDE campaigns enabled the optimal strategy for TEI sampling and provided help for the interpretation of the distribution of TEIs in the subpolar North Atlantic (García-Ibáñez et al., 2015). In addition to the OVIDE line, the Labrador Sea section provided a unique opportunity to study TEI distributions along the boundary current of the western North Atlantic subpolar gyre (Sarthou et al., 2018).

Polonium-210 (^{210}Po, $T_{1/2} = 138.4$ days) and its radioactive grandparent lead-210 (^{210}Pb, $T_{1/2} = 22.3$ years) are two non-conservative ^{238}U decay series products. The GEOTRACES program has included both radionuclides in its TEI list primarily due to ^{210}Po's enhanced bioaccumulation and the use of the ^{210}Po–^{210}Pb pair as a proxy for assessing particle export in the upper ocean. The distribution of ^{210}Po and ^{210}Pb has been widely measured over the last several decades in the Atlantic (e.g., Bacon et al., 1976; Sarin et al., 1999; Rigaud et al., 2015; Ceballos-Romero et al., 2016), Pacific (e.g., Nozaki and Tsunogai, 1976; Murray et al., 2005; Verdeny et al., 2008), Indian (e.g., Cochran et al., 1983; Sarin et al., 1994; Subha Anand et al., 2017), Arctic (e.g., Moore and Smith, 1986; He et al., 2015; Roca-Martí et al., 2016), and Southern oceans (e.g., Shimmield et al., 1995; Friedrich and Rutgers van der Loeff, 2002). However, since the data reported by Bacon et al. (1980b) at the Labrador Sea stations (47.8–53.7° N), there have been few studies of ^{210}Po and ^{210}Pb activity in the North Atlantic at latitudes greater than 40° N. The GEOVIDE cruise, which targeted the North Atlantic from 40 to 60° N, provided an opportunity to fill this data gap.

Besides ascertaining the distribution of the natural radionuclides under specific geographic conditions, this project aimed to answer questions about their biogeochemical behaviors in various marine environments. Owing to the significantly longer half-life of ^{210}Pb relative to ^{210}Po, the two radionuclides are expected to be in secular equilibrium (total ^{210}Po / ^{210}Pb activity ratio = 1) in the ocean, assuming no net removal or addition of either radionuclide. A deficit of ^{210}Po activity relative to ^{210}Pb activity (^{210}Po / ^{210}Pb activity ratio < 1), however, is commonly found in the upper ocean (e.g., Bacon et al., 1976; Nozaki and Tsunogai, 1976; Cochran et al., 1983; Sarin et al., 1999). This has been attributed to a higher particle reactivity of ^{210}Po (higher partitioning coefficient, K_d) than ^{210}Pb in seawater. Particles, therefore, become enriched in ^{210}Po (^{210}Po / ^{210}Pb activity ratio > 1), and their sinking to deeper waters results in a ^{210}Po activity deficit relative to ^{210}Pb activity in the upper water column where particles are formed.

In this work, we describe the distributions of total and size-fractionated particulate ^{210}Po and ^{210}Pb activity along the GEOVIDE cruise in the North Atlantic. These data are a significant contribution to the high-latitude North Atlantic ^{210}Po and ^{210}Pb activity data set. We present a compilation of particulate ^{210}Po / ^{210}Pb activity ratios (ARs) from previous studies in the global ocean, and the results are discussed in regards to the aging of water and biochemical processes. We also describe the relationship among small particles, adsorption, and scavenging of radionuclides. These results lead to recommendations for the estimation of particulate organic carbon (POC) export flux based on the ^{210}Po / ^{210}Pb disequi-

librium, a topic that is covered in a companion paper (Tang et al., 2018).

2 Methods

2.1 Sample collection

The French GEOTRACES cruise to the North Atlantic (GEOVIDE, section GA01; 15 May–30 June 2014) was completed on the R/V *Pourquoi Pas?*. The research vessel departed from Lisbon, Portugal; headed northwest to the Greenland shelf; crossed the Labrador Sea; and ended in St John's, Newfoundland, Canada (Fig. 1). A rosette equipped with conductivity–temperature–depth (CTD) sensors and 12 L Niskin bottles was used to collect 200 seawater samples (5–10 L each) from 10 full-water-column "super" (multicast) stations (16–22 depths per station) and one "XLarge" (five-cast) station to 800 m (station 26, nine depths) for the determination of total ^{210}Po and ^{210}Pb activity. Upon recovery, seawater samples were transferred to 10 L acid-cleaned containers. In addition, particulate radionuclide activities in two size classes (1–53 and > 53 µm) were collected at 3–10 depths per station using large-volume in situ filtration systems (Challenger Oceanic pumps and McLane pumps) equipped with 142 mm filter holders. Each filter head contained a stacked 53 µm PETEX screen followed by a 1 µm pore size quartz fiber QMA filter. The volume filtered was determined via flow meters mounted below each filter head, and the mean volume pumped through each head was 881 L. Once recovered, clear polyethylene caps were placed on the top of the pump heads, and they were brought into a clean laboratory for sub-sampling.

2.2 Total ^{210}Po and ^{210}Pb

Total ^{210}Po and ^{210}Pb activities were determined from the seawater samples by the cobalt–ammonium pyrrolidine dithiocarbamate (Co-APDC) technique (Fleer and Bacon, 1984). Samples were acidified to a pH < 2 with concentrated HCl immediately after collection and spiked with known amounts of ^{209}Po and stable lead as chemical yield tracers. After vigorous stirring and at least 12 h of isotope equilibration, cobalt nitrate and APDC solutions were added to co-precipitate Po and Pb. Samples were filtered through a 0.45 µm membrane filter, and the filters with the precipitate were placed into clean falcon tubes, sealed with Parafilm, and stored in double-bags. As the delay between sample collection and first Po plating increases, the uncertainty of the calculated ^{210}Po activity also increases. In addition, it is necessary to balance counting periods with the number of samples as the uncertainty due to alpha spectrometry counting decreases by increasing the counting time. To limit the delay between sampling and processing and to ensure higher counting statistics by having more alpha spectrometers devoted to this project, sample processing and analyses were split between Universitat Autònoma de Barcelona (UAB; samples from stations 1, 13, and 21) and Queens College (QC; stations 26, 32, 38, 44, 60, 69, and 77). Both laboratories followed the same procedure. Briefly, the filters were digested into a solution of concentrated HNO_3 and HCl; after the solution was evaporated to dryness, the samples were recovered in 1 and 0.5 M HCl solution at UAB and QC, respectively (a 0.5–2 M HCl solution is recommended; Rigaud et al., 2013). A polished pure silver disc (Flynn, 1968) with one side covered by enamel paint was placed into the weak acid solution and heated so that the polonium nuclides were spontaneously plated onto only one side of the disc. The activities of both Po nuclides on the disc were measured by alpha spectrometry. Any ^{210}Po and ^{209}Po remaining in the plating solution were removed using AG 1-X8 anion exchange resin, and the final solution was re-spiked with ^{209}Po and stored for more than 6 months to allow ingrowth of ^{210}Po from the decay of ^{210}Pb.

The ^{210}Pb activity was then determined by re-plating the solutions using silver discs and measuring the ingrown ^{210}Po. Two aliquots of the plating solutions for each sample were taken before the first and second platings for the measurement of total Pb concentration by inductively coupled plasma mass spectrometry (ICP-MS) to determine sample recovery during processing. The average recoveries produced by UAB and QC were 83 ± 11 % ($n = 54$) and 76 ± 14 % ($n = 144$), respectively. The activities of ^{210}Po and ^{210}Pb at the time of collection were determined by a series of corrections, including nuclide decay, ingrowth, chemical recoveries, detector backgrounds, and blank contamination following the methods in Rigaud et al. (2013). The activity uncertainties from UAB were on average 8 % for both ^{210}Po and ^{210}Pb activity, while the QC uncertainties were on average 13 % for ^{210}Po activity and 16 % for ^{210}Pb activity. The greater uncertainties of ^{210}Po and ^{210}Pb activities in the samples processed at QC were due to the longer delay between sampling and first plating (68 vs. 50 days) and higher uncertainties in the determination of the recovery of lead.

2.3 Particulate ^{210}Po and ^{210}Pb

After collection via in situ pumping, one quarter (equivalent to ~ 220 L) of the PETEX screen containing > 53 µm, or "large", particles was processed for radionuclide activity. Swimmers were carefully removed from all samples. The QMA filters containing 1–53 µm, or "small", particles were sub-sampled (two to four punches of 12 mm diameter), achieving a mean effective volume of ~ 66 L. The screens and punches were stored in double bags at -80 °C until the analyses onshore. The particulate samples were split between the two laboratories in parallel to the seawater samples. The filters were spiked with ^{209}Po tracer solution and stable lead, digested using a mixture of concentrated HF, HNO_3, and HCl at UAB, but only HNO_3 and HCl at QC. After multiple rounds of digestion and evaporation to near dryness,

the samples were recovered in 0.5 M HCl solution. Any remaining pieces of filter which were not completely digested were carefully removed, rinsed with 0.5 M HCl solution several times, and then discarded. The analyses of the particulate radionuclide activities were identical to those for the seawater samples described in Sect. 2.2.

2.4 Concentration of suspended particulate matter (SPM)

The Helene Planquette group (University of Brest, co-authors in this issue) collected subsamples from the same screens and filters that were sampled previously for radionuclides to determine major phase composition (particulate organic matter (POM), lithogenic material, calcium carbonate ($CaCO_3$), opal, $Fe(OH)_3$, and MnO_2) (Lam et al., 2015, and references therein). The mass concentration of SPM was calculated as the sum of the chemical dry weight of the major particulate phases.

The calculated SPM concentration was compared to the in situ transmission data obtained from the rosette CTD sensor (Fig. S1 in the Supplement). The overall negative relationship was statistically significant ($R^2 = 0.7$, $n = 53$, $p < 0.0001$), suggesting that the SPM concentrations determined were reasonable estimates of particle concentration in the water column. We used the SPM values to determine the partitioning coefficient, K_d, for ^{210}Po and ^{210}Pb in Sect. 4.4.

2.5 Satellite-based data

The 8-day composites of surface chlorophyll-*a* concentration for each station were retrieved from NASA's MODIS products (https://oceancolor.gsfc.nasa.gov; last access: 6 September 2018) for the period from January to July 2014. The time-series chlorophyll-*a* concentrations were used to show the development of a phytoplankton bloom over time along the transect.

2.6 Historical values

The historical data of the particulate ^{210}Po and ^{210}Pb activity, and the hydrological parameters (pressure, temperature, salinity, and dissolved oxygen) were obtained from databases and publications. The location, date, database address or publication name, and type of data (particulate ^{210}Po and ^{210}Pb activity or hydrological parameters) from all other studies are listed in Table S1 in the Supplement.

2.7 Apparent oxygen utilization

Apparent oxygen utilization ($AOU = O_{2\,saturated} - O_{2\,measured}$) is defined as the difference between the saturated oxygen at a given temperature and salinity and the measured in situ oxygen concentration (Ito et al., 2004; Duteil et al., 2013). A positive AOU indicates either water mass aging and outgassing of oxygen or biological activity, namely respiration (e.g., Keeling et al., 1998; Boyer et al., 1999). Negative AOU, indicating that the water is oversaturated with dissolved oxygen, can appear under the conditions of an intense bloom (e.g., Coppola et al., 2017).

The dissolved oxygen concentration was measured by Winkler titration, and the saturated oxygen concentration was calculated as a function of in situ temperature and salinity, and 1 atm of total pressure based on the built-in function in Ocean Data View (https://odv.awi.de; last access: 6 September 2018).

2.8 Statistical analyses

Statistical analyses were carried out in R Studio version 3 using fitting linear models and Welch two-sample *t* tests. Linear regression analysis was used to investigate the relationship between total particulate ^{210}Po / ^{210}Pb AR and AOU. The Welch two-sample *t* test was applied to assess whether the mean of the total particulate ^{210}Po / ^{210}Pb AR was the same as the mean of the small particulate ^{210}Po / ^{210}Pb AR. It was also applied to investigate the means of the total ^{210}Pb activity in the western and eastern sections along the transect.

3 Results

3.1 Total ^{210}Po and ^{210}Pb activities

Total ^{210}Po activities ($^{210}Po_t$) in all samples ranged from 2.2 to 16.4 dpm 100 L^{-1}, and the mean $^{210}Po_t$ was 8.8 ± 2.4 dpm 100 L^{-1} ($n = 198$, Fig. 2). $^{210}Po_t$ activities were generally low within the mixed-layer and euphotic zone (15–47 m), slightly increased or remained relatively constant in the depth range between the mixed layer and 250 m, and then decreased with water depth at most of the stations except station 26. Near the seafloor, stations 1, 13, and 44 had a slight increase of $^{210}Po_t$ activity.

Total ^{210}Pb activities ($^{210}Pb_t$) were between 2.1 and 20.6 dpm 100 L^{-1} with a mean value of 10.0 ± 3.0 dpm 100 L^{-1} ($n = 198$, Fig. 2). $^{210}Pb_t$ activities were low in the surface, slightly increased in the subsurface, and decreased with water depth. Stations 1, 13, 44, and 60 exhibited an increase near the seafloor.

The mean $^{210}Po_t$ / $^{210}Pb_t$ AR of all samples was 0.92 ± 0.28 ($n = 198$, Fig. 2). When considering different basins separately, there is a tendency of decreasing $^{210}Po_t$ / $^{210}Pb_t$ AR from the West European Basin (1.10 ± 0.35) westwards to the Iceland Basin (0.90 ± 0.19) and the Irminger Sea and the Labrador Sea (0.80 ± 0.18 and 0.83 ± 0.21, respectively).

For all regions, significant deficits of $^{210}Po_t$ (0.80 ± 0.20, $n = 40$) were observed within the mixed-layer and euphotic zone (Fig. 3). Secular equilibrium was also observed at some shallow depths (i.e., 80 m at station 44) and even in surface waters (i.e., 15 m at station 38). $^{210}Po_t$ excesses relative to $^{210}Pb_t$, which were larger than $^{210}Po_t$ surface depletions at the same stations, were observed below the sur-

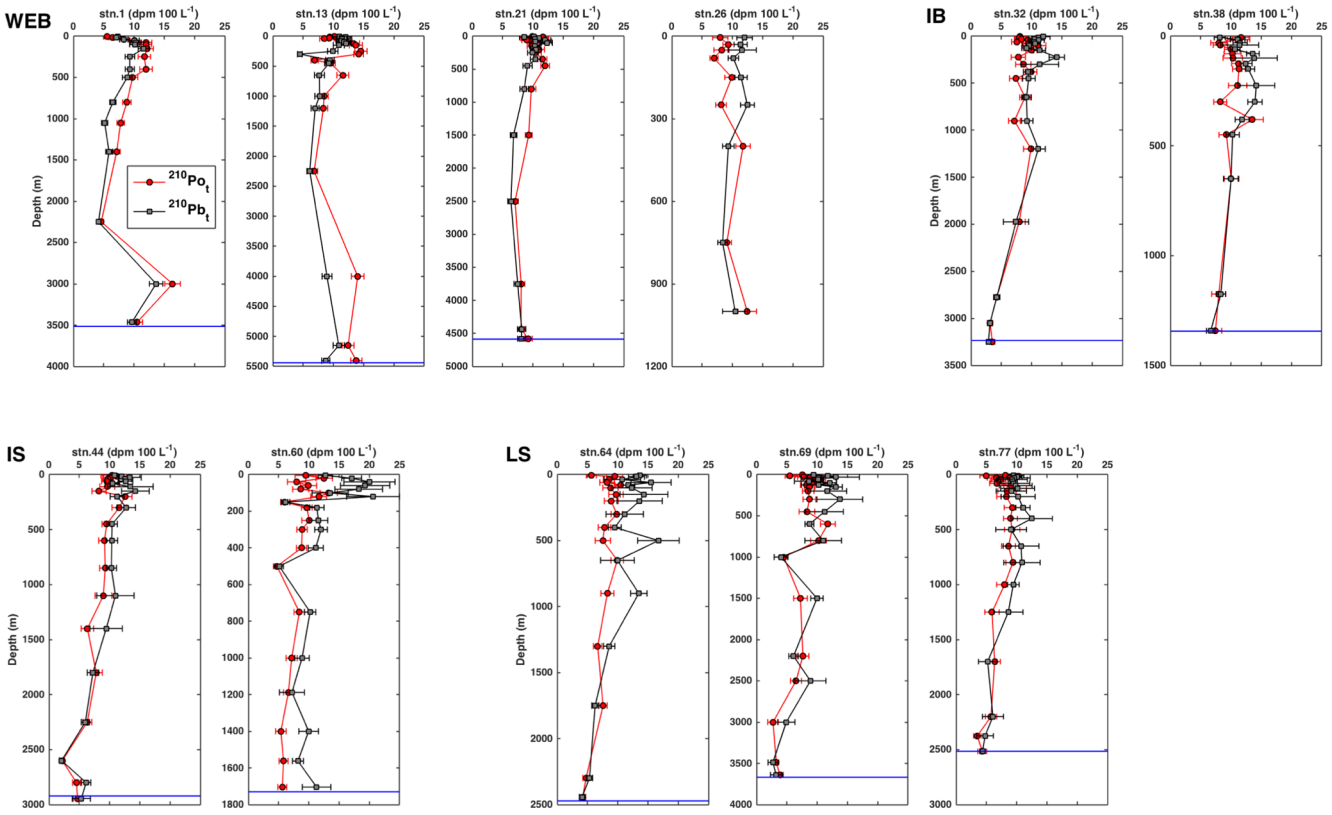

Figure 2. The depth profiles of total ^{210}Po (^{210}Po$_t$, red circles) and ^{210}Pb activities (^{210}Pb$_t$, grey squares) along the GEOVIDE section. The horizontal blue line is the bottom depth, which coincided with the deepest water sample except for station 26, which was sampled only down to 1000 m. Note that the depth scale for each plot may be different. The profiles are shown in the order of sampling date with the region indicated on the top left: West European Basin (WEB), Iceland Basin (IB), Irminger Sea (IS), Labrador Sea (LS).

face at some depths at stations 1, 13, and 21 in the West European Basin (Fig. 2). At depths below the surface to $\sim$ 1500 m in the Iceland Basin, the Irminger Sea, and the Labrador Sea, the water samples still indicated a ^{210}Po deficiency (AR: 0.84 ± 0.17; $n = 27$). Secular equilibrium was generally reached near the bottom depths in all basins except at stations 13 and 60, where the water samples were enriched in ^{210}Po$_t$ (^{210}Po$_t$ / ^{210}Pb$_t$ AR $= 1.58 \pm 0.16$) and depleted in ^{210}Po$_t$ (^{210}Po$_t$ / ^{210}Pb$_t$ AR $= 0.50 \pm 0.12$), respectively.

3.2 Particulate ^{210}Po and ^{210}Pb activities

Small particulate ^{210}Po (^{210}Po$_s$) activities varied in a wide range from 0.08 to 4.82 dpm 100 L^{-1} (mean: 0.76 ± 0.63 dpm 100 L^{-1}; $n = 81$); about 83 % of the values in the small particles were lower than 1.0 dpm 100 L^{-1}, with higher ^{210}Po$_s$ values generally observed in the surface samples (Fig. 4, Table S2). The range of small particulate ^{210}Pb (^{210}Pb$_s$) activities was 0.07 to 2.89 dpm 100 L^{-1} (mean: 0.56 ± 0.46 dpm 100 L^{-1}; $n = 81$). The vertical profiles of ^{210}Pb$_s$ were generally similar to those of ^{210}Po$_s$, with relatively high activity in the surface, lower activity in the subsurface, and increasing activity with depth (Fig. 4). This has been seen in the North Atlantic along the GEOTRACES GA03 transect (Rigaud et al., 2015). The mean ^{210}Po$_s$ / ^{210}Pb$_s$ AR was 1.43 ± 0.96 in the surface waters ($n = 14$, ≤ 47 m) and 1.57 ± 0.90 with all samples included ($n = 81$, 8–3440 m). While most surface observations had an AR of ^{210}Po$_s$ / ^{210}Pb$_s$ higher than unity, five surface samples at stations 69 and 77 showed an enrichment of ^{210}Pb activity over ^{210}Po (^{210}Po$_s$ / ^{210}Pb$_s$ AR: 0.62 ± 0.18).

Large particulate ^{210}Po (^{210}Po$_l$) activities ranged from 0.01 to 0.83 dpm 100 L^{-1} with a mean of 0.10 ± 0.12 dpm 100 L^{-1} ($n = 59$, Fig. 5, Table S2). The range of ^{210}Pb activity in the large particles (^{210}Pb$_l$) was from 0.02 to 0.67 dpm 100 L^{-1} (mean: 0.12 ± 0.14 dpm 100 L^{-1}; $n = 59$). The highest ^{210}Po$_l$ and ^{210}Pb$_l$ values were found at 30 m at station 26. The mean ^{210}Po$_l$ / ^{210}Pb$_l$ AR was 1.09 ± 1.54 in the surface waters ($n = 14$, ≤ 47 m) and 1.06 ± 0.86 when all data were considered ($n = 59$, 8–800 m). There were 17 % of the samples with a depletion of ^{210}Po activity relative to ^{210}Pb activity in large particles (mean AR: 0.49 ± 0.23), particularly in surface waters from the western section. We address this issue further in Sect. 4.2 and 4.3.

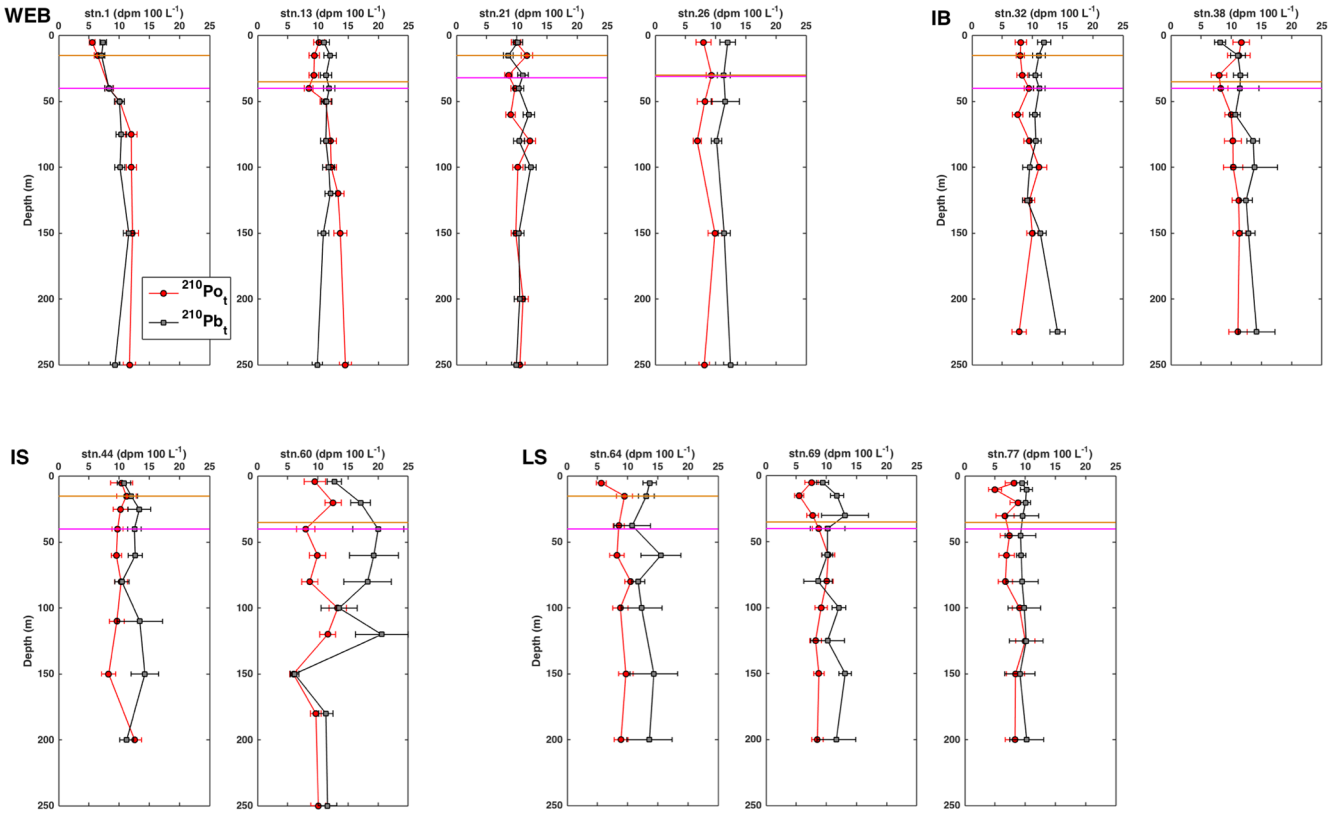

Figure 3. The upper 250 m of the depth profiles of total ^{210}Po (^{210}Po$_t$, red circles) and ^{210}Pb activities (^{210}Pb$_t$, grey squares) along the GEOVIDE section. The horizontal orange and magenta lines denote the mixed-layer depth (MLD) and the base of the euphotic zone ($Z_{1\,\%}$), respectively. The depth profiles are shown in the order of sampling and grouped by region (refer to Fig. 2 for the text abbreviations).

The percentages of total ^{210}Po activity in the small and large particles ranged from 0.9 % to 46.7 % (mean: 8.0 ± 6.7 %) and from 0.1 % to 8.9 % (mean: 1.2 ± 1.5 %), respectively. The percentage of total ^{210}Pb activity ranged from 0.7 % to 21.4 % (mean: 4.9 ± 3.8 %) and from 0.2 to 5.9 % (mean: 1.1 ± 1.2 %) in the small and large particulate phase, respectively. These values revealed that both radionuclides were predominantly present in the dissolved phase along this transect, as is commonly found in the ocean. The particulate percentages reported here are similar to the values reported from the FS "Meteor" cruise 32 in the North Atlantic (Bacon et al., 1976) and along the North Atlantic GA03 transect (Rigaud et al., 2015).

We then combined radionuclide activity on the small and large particles from the same depth as the total particulate activity. There were 56 samples in total (surface to 800 m), and 41 of them were from the upper 200 m. Most of the total particulate ^{210}Po (^{210}Po$_p$) and ^{210}Pb (^{210}Pb$_p$) activity was on the small particles, with 86 % of ^{210}Po$_p$ and 80 % of ^{210}Pb$_p$ on the small size fraction (data not shown). The total particulate ^{210}Po and ^{210}Pb AR (^{210}Po$_p$ / ^{210}Pb$_p$) had the same mean as that of the small particulate ^{210}Po and ^{210}Pb AR (^{210}Po$_s$ / ^{210}Pb$_s$) (Welch two-sample t test, $n = 56$, $p = 0.1$), indicating that the values of the ^{210}Po$_p$ / ^{210}Pb$_p$ activity ratios were driven by the small particles. While the majority of particulate matter was enriched in ^{210}Po (^{210}Po$_p$ / ^{210}Pb$_p$ AR > 1), there were 13 out of 56 total samples from various depths that were depleted in ^{210}Po relative to ^{210}Pb. The ^{210}Po$_p$ / ^{210}Pb$_p$ activity ratios from this study are compared to the results from previous studies in various oceanic regimes in Sect. 4.2.

4 Discussion

4.1 Total ^{210}Po and ^{210}Pb activities

The overall profiles of ^{210}Po$_t$ and ^{210}Pb$_t$ activities were different among basins (Fig. 2). The deficiencies of ^{210}Po$_t$ activities with respect to ^{210}Pb$_t$ activities in the surface samples from the Iceland Basin, the Irminger Sea, and the Labrador Sea were generally greater than those from the West European Basin. Such disequilibria generally extended to the deep waters (1700–2950 m). In contrast, ^{210}Po$_t$ activities in the West European Basin were generally enriched relative to ^{210}Pb$_t$ activities from below the surface to the bottom of the profile. In the West European Basin, the subsurface ^{210}Po$_t$ activity excess was much larger than the surface depletion, sug-

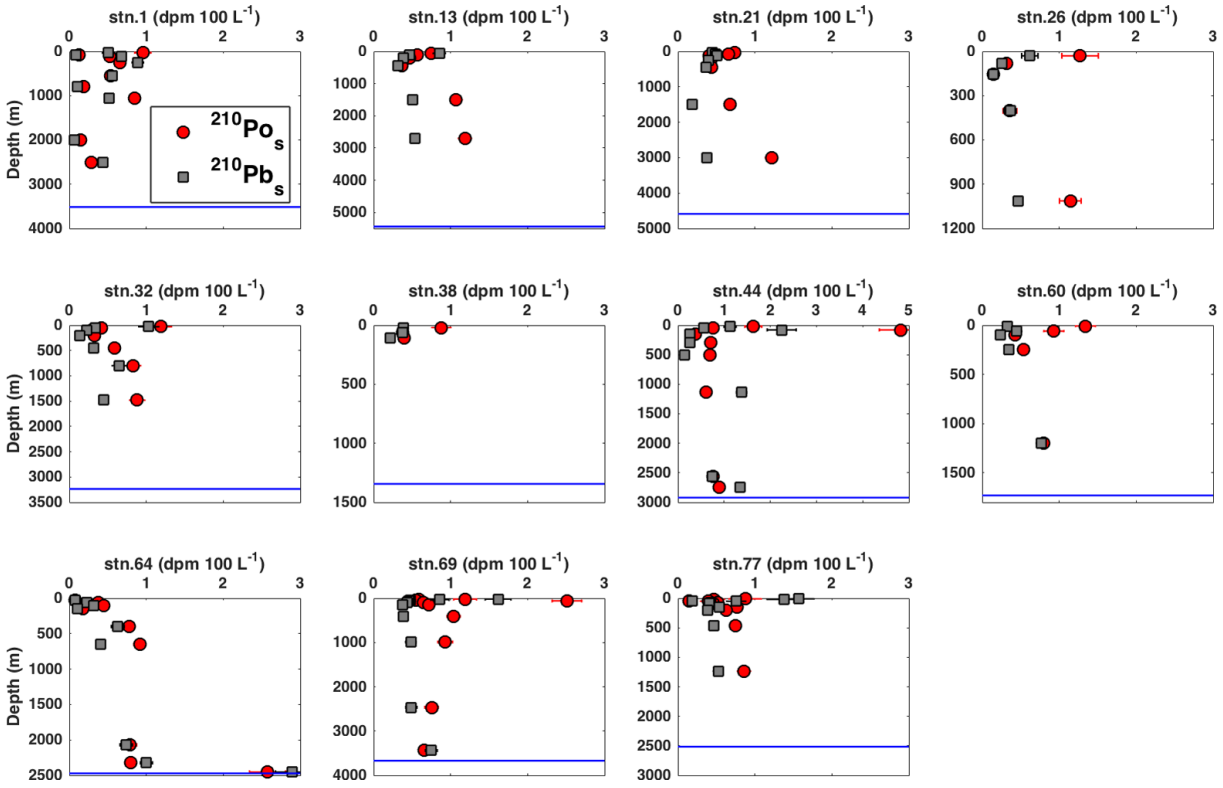

Figure 4. Vertical profiles of the particulate ^{210}Po and ^{210}Pb activity in the small size fraction (1–53 µm, $^{210}Po_s$, $^{210}Pb_s$). Note that the depth scale may differ among plots, and the activity scale at station 44 differs from the scale in all other plots. The horizontal blue line represents the bottom depth at that station.

gesting that some external source would be needed to maintain this excess ^{210}Po activity within the water column. One possible source of these subsurface ^{210}Po activity excesses below 2000 m at stations 1 and 13 could be the lower Northeast Atlantic Deep Water ($NEADW_L$), which was the dominant water mass in the Iberian Basin from 2000 m to the bottom and had a concentration of silicate up to 48 µmol kg^{-1} (García-Ibáñez et al., 2015). High activity of ^{210}Po in deep samples could be due to the dissolution of diatoms or herbivore feces (Cooper, 1952). As these particles sink and dissolve, ^{210}Po activity may have been preferentially released to the dissolved phase compared to ^{210}Pb activity (Bacon et al., 1976), leading to ^{210}Po excess observed in the deep waters at stations 1 and 13. For the subsurface ^{210}Po activity excesses at station 1 between 400 and 1000 m, where lateral inputs of particulate Fe (PFe) from the margin was observed (Gourain et al., 2018), the likely process is diffusion of ^{210}Po from those particles originated from the margin, and such excess could be transported westwards to station 13 by lateral advection. An alternative source of ^{210}Po activity excess between 50 and 250 m at stations 1 and 13 (Fig. 3) could be the eastern boundary upwelling along the coast of the Iberian Peninsula (García-Ibáñez et al., 2015). Even though no strong upwelling events were revealed from temperature and density profiles during the cruise, northerly winds favoring upwelling were recorded 2–3 months before the sampling (Shelley et al., 2017). The deep water may have excess ^{210}Po activity due to the remineralization of sinking particles. The upwelling of this water mass prior to the sampling date could maintain such subsurface excess ^{210}Po activity. Similar findings have been reported in the Cariaco Trench for the upper 300 m of the water column by Bacon et al. (1980a).

As atmospheric deposition is the main source of ^{210}Pb to the water column (e.g., Masqué et al., 2002), we divided the GA01 transect into a western section (stations 44–77) and an eastern section (stations 1–38) based on atmospheric deposition boxes described in Shelley et al. (2017). Total atmospheric deposition fluxes of a suite of aerosol-sourced trace metals (TEs) were reported to be higher in the east than the west for 18 out of 19 TEs (Shelley et al., 2017). However, a two-sample t test revealed a greater mean of $^{210}Pb_t$ activity in surface waters in the western than in the eastern section ($p < 0.02$; mean: 12.1 vs. 10.4 dpm 100 L^{-1}), despite the fact that ^{210}Pb is usually associated with aerosols. Even though the direct input of atmospheric ^{210}Pb may be larger in the east (assuming it behaves like the other trace metals, but without aerosol ^{210}Pb data we cannot confirm this), alternative inputs of ^{210}Pb from freshwater (e.g., sea ice processes and meteoric water) could be a greater source of ^{210}Pb activity to the west. The freshwater sources over the Greenland

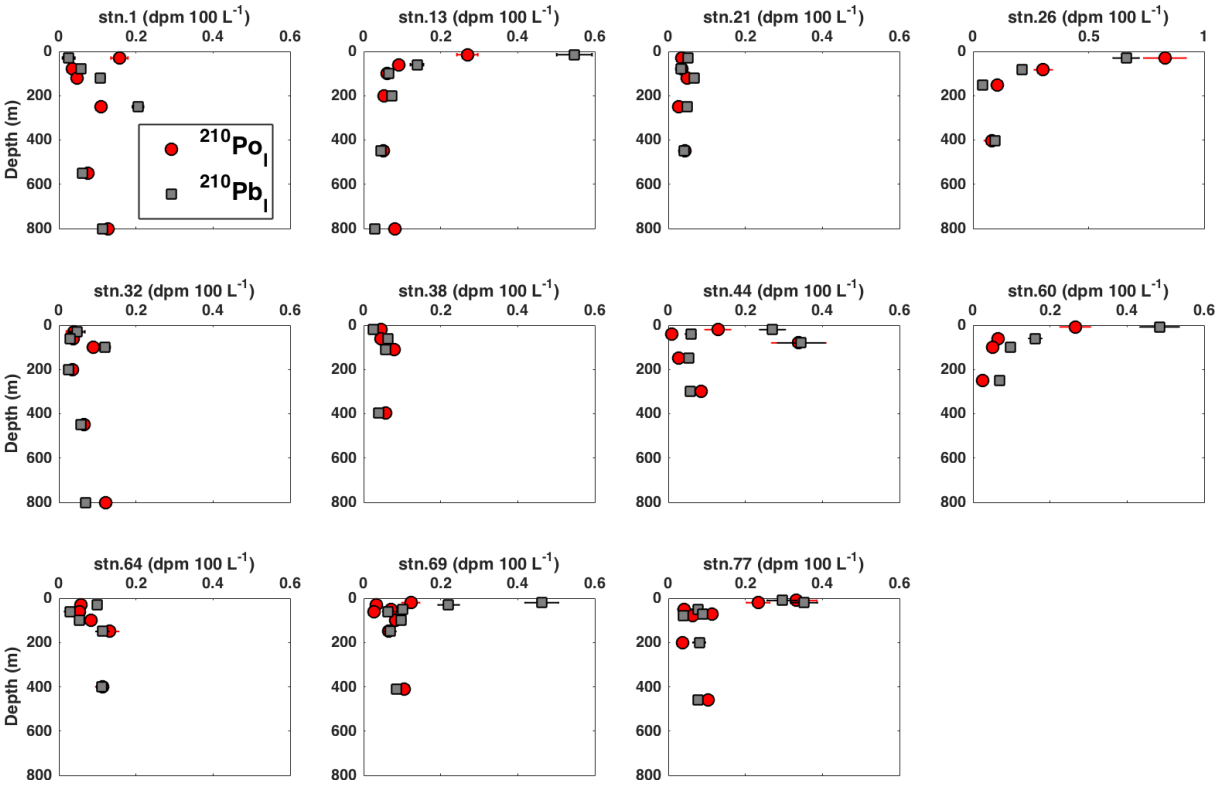

Figure 5. The vertical profiles of the particulate ^{210}Po and ^{210}Pb activity in the large size fraction (> 53 µm, ^{210}Po$_l$, ^{210}Pb$_l$) in the top 800 m. Note that the activity scale at station 26 differs from the scale in all other plots.

shelf and slope have been identified by Benetti et al. (2017) and were believed to be an important source of Fe (Tonnard et al., 2018) and Al (Menzel Barraqueta et al., 2018) off of Greenland during this cruise. This result highlights the need in the future to measure ^{210}Pb activity simultaneously in the atmospheric and local freshwater sources in order to account for all source terms.

4.2 Total particulate ^{210}Po / ^{210}Pb AR

A proposed explanation for the depletion of ^{210}Po activity relative to ^{210}Pb activity (AR < 1) in some particles is effective recycling, commonly characterized by a subsurface excess of dissolved ^{210}Po activity released from enriched particles leaving the surface. Bacon et al. (1976) suggested that the efficiency of this recycling could reach up to 50 %, while there is no significant concurrent release of ^{210}Pb activity in the water column. Laboratory studies have found the release rate of ^{210}Po in marine particulate matter to be significant; for example, 41 % of the ^{210}Po activity in euphausiid fecal pellets was released over 5 days as presented in Heyraud et al. (1976). An alternative explanation for the depletion of ^{210}Po activity in particles is their lithogenic origin. ^{210}Po / ^{210}Pb AR in lithogenic particles was reported to be similar to or less than unity (Nozaki et al., 1998; Tateda et al., 2003). In addition, the AR < 1 observed at station 1 (120, 250, and 550 m) could be associated with lithogenic particles from the Iberian Margin, where 100 % of the PFe had a lithogenic origin, while the lithogenic contribution to PFe at other stations was smaller (Gourain et al., 2018).

The time-series chlorophyll-*a* concentrations (8-day composite; https://oceancolor.gsfc.nasa.gov, last access: 6 September 2018) from January to July 2014 at each station revealed bloom conditions about 4 months prior to the sampling time (Fig. 6). We estimated the days since the last bloom began prior to the sampling date for each station (Table 1) and put these data into the context of the low ^{210}Po$_p$ / ^{210}Pb$_p$ AR (< 1) in the total particles > 1 µm (Fig. 7). Eight stations had total particulate samples with ^{210}Po$_p$ / ^{210}Pb$_p$ AR lower than unity from either shallow or deep waters. Specifically, when the time since the last bloom began was relatively short (25–47 days), the samples with ^{210}Po$_p$ / ^{210}Pb$_p$ AR < 1 were observed in the shallow waters (10–60 m). In contrast, when more time (50–74 days) had passed since the last bloom, the depths at which samples had ^{210}Po$_p$ / ^{210}Pb$_p$ AR < 1 were found to be much deeper (120–500 m). The results indicated that post-bloom particles could be recycled for weeks in shallow depths and take weeks to months to sink to deeper waters.

The averages of ^{210}Po$_p$ / ^{210}Pb$_p$ AR within the upper 200 m water column were put into a global context with previously reported results (Fig. 8). Total particulate

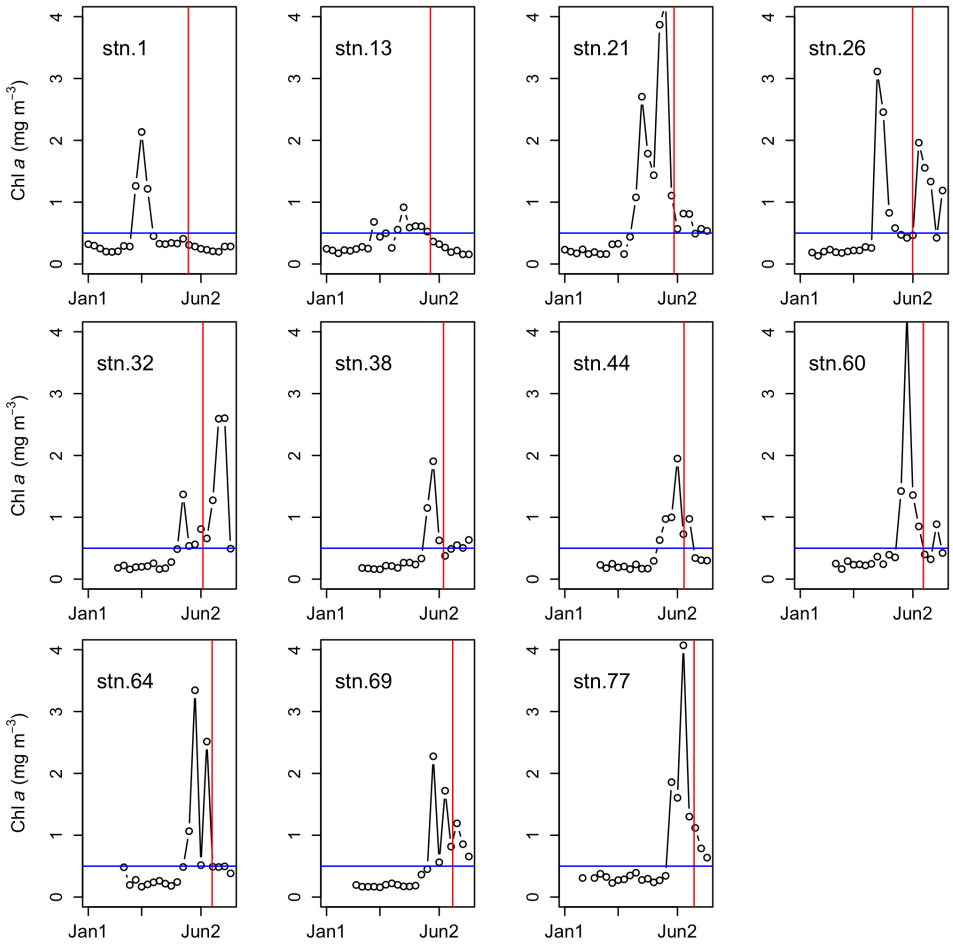

Figure 6. Time-series (1 January–12 July 2014) chlorophyll-*a* concentrations (8-day averages) from Aqua MODIS (https://oceancolor.gsfc.nasa.gov; last access: 6 September 2018) at each station along the GA01 transect. The vertical red line denotes the sampling date at each station. The horizontal blue line denotes chlorophyll-*a* concentration of 0.5 mg m^{-3}. The time when chlorophyll-*a* concentration first exceeded 0.5 mg m^{-3} after the end of the last bloom defines the date when the next bloom began.

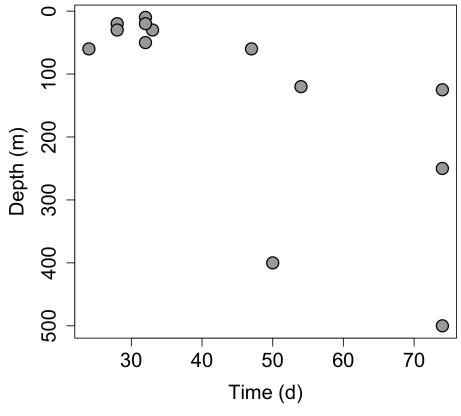

Figure 7. Depths at which the total particulate (> 1 µm) ^{210}Po / ^{210}Pb activity ratio was lower than unity vs. the time since the last bloom (data are presented in Table 1).

^{210}Po / ^{210}Pb ARs in the open ocean in previous studies (e.g., equatorial western Pacific, Bellingshausen Sea, Bermuda Atlantic Time-series Study (BATS) site, Labrador Sea) were generally greater than unity. In contrast to the open ocean, the data show a distinct trend of depletion of relative ^{210}Po activity in marine particles from the shallow seas of the high-latitude Northern Hemisphere. The lowest total particulate ^{210}Po / ^{210}Pb AR values (Table 2, 0.4–0.5) were found in the Chukchi shelf (He et al., 2015) and other seas from the Eurasian sector (Barents, Kara, and Laptev seas) as well as in central Arctic (Friedrich, 2011). Previous studies have observed depletion of relative ^{210}Po activity in nearshore particles in the Yellow Sea (Hong et al., 1999); in the turbid waters off of western Taiwan (Wei et al., 2012); on the shelf of Woods Hole, MA, USA (Rigaud et al., 2015); and now in the margin station off St. John's, Canada (this study). The previous authors attributed the relative depletion of particulate ^{210}Po activity in the nearshore waters to the terrestrial origin/riverine input of particles with a low ^{210}Po / ^{210}Pb

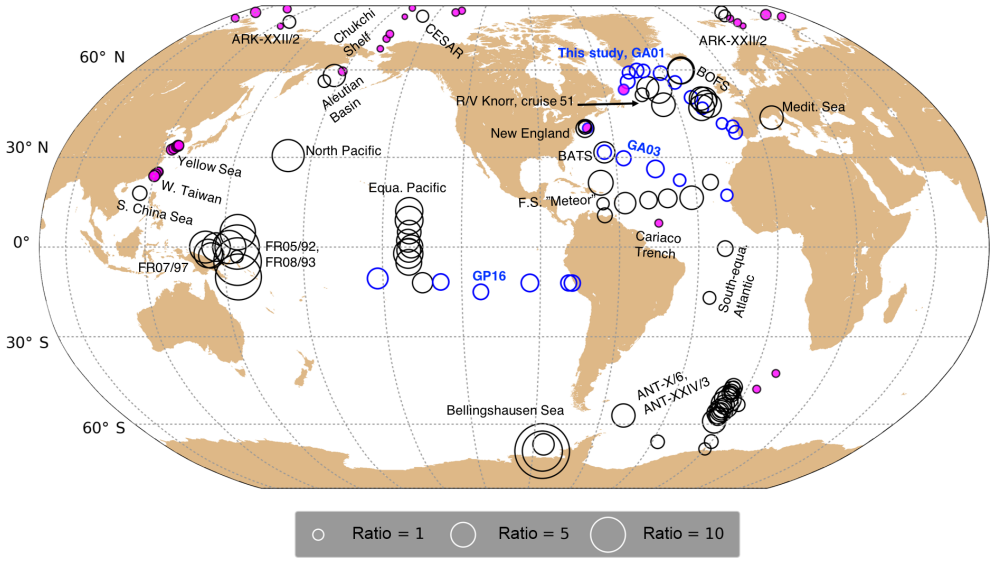

Figure 8. Comparison of particulate ^{210}Po / ^{210}Pb activity ratios in the upper 200 m from this study and 20 previous studies (references in Table 2). Information about the study site, sampling date, method, and particle size of each study is shown in Table 2. The black circles represent data from previous studies, while the blue circles are the results from samples analyzed at QC from three recent GEOTRACES transects (GA03; GP16; and this study: GA01 GEOVIDE). The filled magenta and open circles indicate activity ratios lower and higher than 1, respectively.

AR. This may partially explain low activity ratios in the samples from the shelf of the Arctic Ocean as well, since it receives $\sim 10\,\%$ of global river runoff and is the most riverine-influenced of all of the world's oceans (Opsahl et al., 1999; Carmack et al., 2006). The Arctic Basin, similarly, had widespread deficits of particulate ^{210}Po activity in the upper water column during the sea ice minimum in 2007 (Roca-Martí et al., 2018). Besides shelf particles, the authors suggest that other particle types could also play a role in lowering the particulate AR, including sea ice sediments, remineralized material, fecal pellets, and picoplankton aggregates.

4.3 Relationship between total particulate ^{210}Po / ^{210}Pb AR and AOU

AOU is a time-integrated measure of the amount of oxygen removed during the biogeochemical processes (e.g., respiration, remineralization, oxidation) in the ocean interior. Therefore, AOU is a product of apparent oxygen utilization rate (AOUR) and the age of water mass (e.g., Stanley et al., 2012); i.e., high AOU could be due to either intense biogeochemical processes that have occurred in a short period of time (young water mass) or weaker processes over a longer period of time (old water mass). Consequently, the rate of these biogeochemical processes and time (water mass age) would have different or similar impacts on the ^{210}Po$_p$ / ^{210}Pb$_p$ AR value depending on the initial AR in the particles and the natural of the particles. For example, the ^{210}Po$_p$ / ^{210}Pb$_p$ AR would tend to increase with time if the initial AR were < 1 because particulate ^{210}Po activity would increase from the decay of ^{210}Pb and trend towards secular equilibrium (^{210}Po$_p$ / ^{210}Pb$_p$ AR $= 1$), and to decrease with time if the initial AR were > 1 as the original excess of particulate ^{210}Po activity would disappear after seven half-lives of ^{210}Po. In contrast, oxygen consumption due to bacterial remineralization would preferentially release ^{210}Po activity from particles into the dissolved pool (e.g., Stewart et al., 2008), leading to a lower ^{210}Po$_p$ / ^{210}Pb$_p$ AR in those particles.

The combination of average ^{210}Po$_p$ / ^{210}Pb$_p$ AR and their corresponding average AOU in the upper 200 m at 40 stations from four independent studies – including ARK-XXII/2 (77.38–87.83° N, $n = 15$) in the Arctic and BOFS (48.89–49.87° N, $n = 7$), GA03 (22.38–39.70° N, $n = 7$), and GA01 (this study; 40.33–59.80° N, $n = 11$) in the North Atlantic (see map in Fig. 8) – suggests two distinct linear trends (Fig. 9). When AOU was lower than 25 µmol kg^{-1}, the ^{210}Po$_p$ / ^{210}Pb$_p$ AR was found to be greater than unity, together with a linear negative relationship ($n = 27$, $R^2 = 0.5$, $p < 0.001$) towards the AOU at 25 µmol kg^{-1}. In contrast, AOU values greater than 25 µmol kg^{-1} were coincident with a ^{210}Po$_p$ / ^{210}Pb$_p$ AR < 1, and a linear positive relationship ($n = 12$, $R^2 = 0.4$, $p = 0.03$) towards the highest AOU values was measured. The two contradictory linear trends likely reflect the nature of the particles. For example, the observation of ^{210}Po$_p$ / ^{210}Pb$_p$ AR > 1 with AOU < 25 µmol kg^{-1} may suggest relatively fresh/organic particles in the young water mass. When AOU increases due to either water mass aging or higher AOUR, the ^{210}Po$_p$ / ^{210}Pb$_p$ AR decreases with a slope of -0.17 ± 0.04. On the other hand, refrac-

Table 1. Biological characteristics of the water column determined by chlorophyll-*a* concentration (8-day composite) from Fig. 6, including the date when the last bloom began, the difference in chlorophyll-*a* concentration between the sampling time and last bloom peak, and the days since the last bloom. Activity ratios of $^{210}Po_p$ / $^{210}Pb_p$ < 1 and their corresponding depths are also shown. NA indicates that all samples from the corresponding depth range had $^{210}Po_p$ / $^{210}Pb_p$ equal to or greater than 1 (no sample with $^{210}Po_p$ / $^{210}Pb_p$ < 1).

Station	Sampling date	The date last bloom began	Last bloom peak–current state	Days since last bloom	$^{210}Po_p$ / $^{210}Pb_p$ < 1	
					0–100 m	> 100 m
1	19 May 2014	6 Mar 2014	Large	74	NA	Yes (120, 250, 500 m)
13	24 May 2014	7 Apr 2014	Small	47	Yes (60 m)	NA
21	1 Jun 2014	7 Apr 2014	Large	55	NA	Yes (120 m)
26	4 Jun 2014	15 Apr 2014	Large	50	NA	Yes (400 m)
32	8 Jun 2014	9 May 2014	Small	30	NA	NA
38	11 Jun 2014	17 May 2014	Small	25	Yes (60 m)	NA
44	13 Jun 2014	9 May 2014	Small	35	NA	NA
60	18 Jun 2014	17 May 2014	Large	32	NA	NA
64	20 Jun 2014	17 May 2014	Small	34	Yes (30 m)	NA
69	22 Jun 2014	25 May 2014	Small	28	Yes (20, 30 m)	NA
77	26 Jun 2014	25 May 2014	Small	32	Yes (10, 20, 50 m)	NA

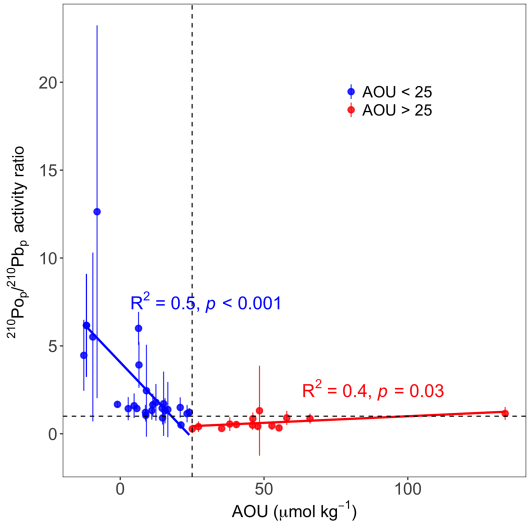

Figure 9. The relationship between AOU (μmol kg^{-1}) and total particulate ^{210}Po / ^{210}Pb activity ratio ($^{210}Po_p$ / $^{210}Pb_p$) from the upper 200 m in the Northern Hemisphere (> 22° N) investigated by a linear regression model (red and blue lines). The 40 stations include data from previous studies – ARK-XXII/2 (77.38–87.83° N, n = 15) in the Arctic and BOFS (48.89–49.87° N, n = 7), GA03 (22.38–39.70° N, n = 7), and GA01 (this study; 40.33–59.80° N, n = 11) – in the North Atlantic. The horizontal dashed line represents $^{210}Po_p$ / $^{210}Pb_p$ AR = 1, and the vertical dashed line represents AOU = 25 μmol kg^{-1}. Blue circles denote AOU < 25 μmol kg^{-1}, while red circles denote AOU > 25 μmol kg^{-1}.

tory/lithogenic particles may be suggested by the observation of $^{210}Po_p$ / $^{210}Pb_p$ AR < 1 with AOU > 25 μmol kg^{-1}. For those particles, increasing in AOU due to either water mass aging or higher AOUR would change the $^{210}Po_p$ / $^{210}Pb_p$ AR to a much lesser degree than that for organic particles with a slope of 0.008 ± 0.003. This explanation, however, appears to only hold for the high-latitude Northern Hemisphere, where $^{210}Po_p$ / $^{210}Pb_p$ activity ratios were generally lower than those in the other oceanic settings (Fig. 8). In the high-latitude Southern Hemisphere near Antarctic (e.g., ANT-X/6), for example, there is no apparent relationship between $^{210}Po_p$ / $^{210}Pb_p$ activity ratios and AOU. This relationship (or lack thereof) deserves more study in the future.

4.4 Relationship among small particles, adsorption, and scavenging

The partitioning coefficient, K_d (L kg^{-1}), has been used to describe the particle adsorption behavior of radionuclides. It is defined as the ratio of the adsorbed radionuclide activity (A_p, dpm 100 L^{-1}) to the dissolved radionuclide activity (A_d, dpm 100 L^{-1}), normalized by the SPM concentration (μg L^{-1}):

$$K_d = \frac{A_p}{A_d} \times \frac{1}{\mathrm{SPM}} 10^9. \quad (1)$$

Owing to the different biological and chemical behaviors of ^{210}Po and ^{210}Pb, the interpretation of measured K_d for ^{210}Po (K_d(Po)) may not be as clear as that for ^{210}Pb (K_d(Pb)). As claimed previously in Tang et al. (2017), K_d(Po) is complicated because it appears to reflect both the surface adsorption and potential bioaccumulation.

In this study, the size-fractionated data of both radionuclide activity and SPM allowed us to calculate the partitioning coefficients for both radionuclides on small and total particles. The dissolved radionuclide activity was calculated as the difference between total and particulate activity. The coefficients for the small particulate and the total particulate phases were normalized by the SPM in the small and total particulate phases, respectively. We present the coef-

Table 2. The compilation of total particulate ^{210}Po / ^{210}Pb activity ratios ($^{210}Po_p$ / $^{210}Pb_p$) averaged in the upper 200 m, including this study.

Region		Sampling method	Date	Size (µm)	Depth (m)	$^{210}Po_p$ / $^{210}Pb_p$	Reference
Arctic	CESAR	In situ pump	Apr–May 1983	> 0.45	2–200	1.2 ± 0.7	Moore and Smith (1986)
	Arctic (ARK-XXII/2)	Niskin bottle	Jul–Sep 2007	> 1	10–200	0.50 ± 0.20	Friedrich (2011)
	Chukchi Shelf	Niskin bottle	Jul–Sep 2010	> 0.45	0–90	0.37 ± 0.10	He et al. (2015)
Atlantic	F.S. Meteor	Niskin bottle	Nov–Dec 1973	> 0.4	0–200	3.1 ± 1.4	Bacon (1977)
	Cariaco Trench	Niskin bottle	Dec 1973	> 0.4	0–200	1.4 ± 0.6	Bacon et al. (1980a)
	Labrador (R/V *Knorr*)	Niskin bottle	Jun 1975	> 0.4	0–100	3.9 ± 1.5	Bacon et al. (1980b)
	South of New England	Niskin bottle	Jul 1980	> 0.45	4–200	1.8 ± 0.8	Bacon et al. (1988)
	N. Atlantic (BOFS)	Niskin bottle	May–Jun 1989, 1990	> 0.45	0–150	6.0 ± 4.5	BODC et al. (2016)
	Equa. South Atlantic	Niskin bottle	May–Jun 1996	> 0.7	10–200	1.3 ± 1.1	Sarin et al. (1999)
	BATS	Go-Flo bottle	Oct 1996	> 0.45	0–200	3.7 ± 3.2	Kim and Church (2001)
	N. Atlantic (GA03)	In situ pump	Oct–Nov 2010, Nov–Dec 2011	> 0.8	30–200	1.5 ± 0.5	Rigaud et al. (2015)
	N. Atlantic (GA01)	In situ pump	May–Jun 2014	> 1	8–200	1.4 ± 0.3	This study
Pacific	North Pacific	Niskin bottle	Nov 1973	> 0.4	10–150	8.5 ± 5.7	Bacon et al. (1976)
	W. Pacific (FR05/92)	Niskin bottle	Jul 1992	> 0.45	0–200	1.3 ± 1.0	Towler (2003)
	Equa. Pacific	Go-Flo bottle	Aug–Sep 92	> 0.45 or 0.5	0–200	5.1 ± 1.2	Murray et al. (2005)
	W. Pacific (FR08/93)	Niskin bottle	Nov 1993	> 0.45	0–200	16 ± 4	Towler (2013)
	W. Pacific (FR07/97)	Niskin bottle	Aug 1997	> 0.45	0–200	7.2 ± 1.5	Peck and Smith (2002)
	Aleutian Basin	Niskin bottle	Jul–Aug 2008	> 0.2	0–200	1.9 ± 3.0	Hu et al. (2014)
	E. Pacific (GP16)	In situ pump	Oct–Dec 2013	> 1	15–200	2.4 ± 0.6	Unpublished
Antarctic	S. Ocean (ANT-X/6)	Niskin bottle	Oct–Nov 92	> 0.45	20–200	3.0 ± 1.4	Smetacek et al. (1997)
	Bellingshausen Sea	Go-Flo bottle	Nov–Dec 1992	> 0.45	0–100	14 ± 11	Shimmield et al. (1995)
	S. Ocean (ANT-XXIV/3)	Niskin bottle	Feb–Apr 2008	> 0.45	25–200	1.3 ± 0.9	Friedrich et al. (2011)
Margin Sea	S. China Sea	Go-Flo bottle	Jan–Oct 2007, May 2008	> 0.45	0–200	1.7 ± 1.1	Wei et al. (2014)
	W. Taiwan	Go-Flo bottle	Apr 2007	> 0.45	8–25	0.85 ± 0.12	Wei et al. (2012)
	Yellow Sea	Niskin bottle	Feb 1993	> 0.7	0–100	0.88 ± 0.08	Hong et al. (1999)
	Mediterranean Sea	Sediment trap	Mar–Jun 2003		200	4.5 ± 1.0	Stewart et al. (2007)

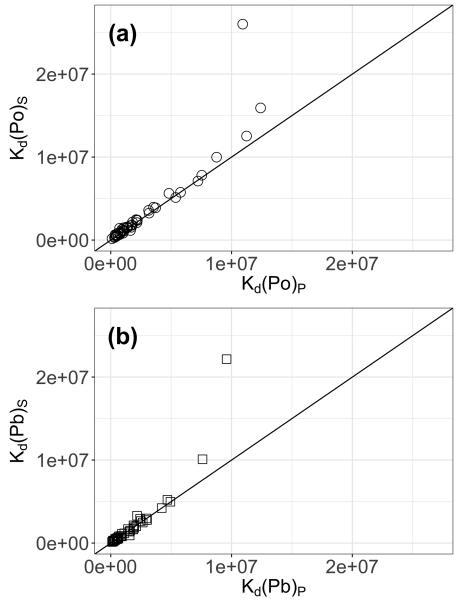

Figure 10. Comparison of the partitioning coefficient (K_d, L kg^{-1}) between the dissolved and small particulate phases ($K_d(Po)_s$, $K_d(Pb)_s$) vs. between the dissolved and total particulate phases ($K_d(Po)_p$, $K_d(Pb)_p$) for **(a)** ^{210}Po and **(b)** ^{210}Pb. The 1 : 1 line is indicated as the solid line in each plot.

ficients for the small particulate phases ($K_d(Po)_s$, $K_d(Pb)_s$) and the total particulate phases ($K_d(Po)_p$, $K_d(Pb)_p$) because most of the particulate activity (> 80 %) was associated with the small particles along the GEOVIDE transect, and most conceptualized scavenging models consider either the two-box model (dissolved–total particulate phases, i.e., $K_d(Po)_p$) or the three-box model (dissolved–small–large, i.e., $K_d(Po)_s$) (Clegg and Whitfield, 1990, 1991; Rigaud et al., 2015), and thus activity is concentrated from the dissolved phase to the total or small particles.

The average values of K_d(Po) were 1.6 times of those of K_d(Pb) in both small and total particulate phases, suggesting a higher affinity with particles for ^{210}Po with respect to ^{210}Pb, which is commonly observed in the global ocean (Bacon et al., 1988; Hong et al., 1999; Masqué et al., 2002; Wei et al., 2014; Tang et al., 2017). The K_d values for the small particulate phase were slightly higher than those for the total particulate phase, but overall these values were very similar for both radionuclides (Fig. 10), suggesting that adsorption/scavenging of radionuclides was driven by small particles along the transect. In addition, there are increasing studies which argue that small particles can form aggregates that sink, and their contribution to carbon export could be larger than previously thought (e.g., Richardson and Jackson, 2007; Lomas and Moran, 2011; Amacher et al., 2013; Puigcorbé et al., 2015). We, therefore, recommend combining the activities of both small and large particles into a total particulate fraction in order to explain total ^{210}Po / ^{210}Pb disequilibria in the surface waters, and utilizing the characteristics of the total particles (instead of just the large particles) in the estimation of the POC export fluxes (Tang et al., 2018).

Traditionally, large particles collected by in situ filtration with pumps, most commonly defined as particles larger than 53 or 70 µm, were assumed to dominate the sinking flux (Dugdale and Goering, 1967; Bishop et al., 1977; Fowler and Knauer, 1986; Honjo et al., 1992; Walsh and Gardner, 1992) such that the composition (POC / ^{210}Po) of the large particle size class was used to convert ^{210}Po fluxes into POC export (e.g., Friedrich and Rutgers van der Loeff, 2002; Cochran and Masqué, 2003; Murray et al., 2005; Stewart et al., 2010; Roca-Martí et al., 2016). Given that the true size spectrum of sinking particles for the timescale relevant to the ^{210}Po / ^{210}Pb method is unknown and the POC flux estimates are sensitive to the particulate POC / ^{210}Po ratio, both small and large particles should be sampled for POC / ^{210}Po due to the variability in the POC / ^{210}Po ratio in different size classes (Hayes et al., 2018).

5 Conclusions

In this study, we reported the vertical distribution of total and size-fractionated particulate ^{210}Po and ^{210}Pb activities in the North Atlantic during the GEOVIDE GA01 cruise. More than 90 % of the radionuclide activity was found in the dissolved phase, while a small proportion was associated with particles in this transect. Total ^{210}Po activity was generally depleted relative to total ^{210}Pb activity in the upper 100 m due to the preferential adsorption of ^{210}Po activity by particles. Such deficiencies of ^{210}Po activities generally extended to the deep waters at most of the stations. In the West European Basin, the excess of ^{210}Po activities at stations 1 and 13 in the Northeast Atlantic Deep Water was attributed to the release of ^{210}Po during dissolution of sinking biogenic particles.

There appear to be geographic differences in particulate ^{210}Po / ^{210}Pb activity ratios measured during GEOVIDE and previous studies, with particularly low values in the high-latitude North Atlantic and Arctic. While this observation deserves more attention, we support previous suggestions that this is due to the terrestrial origin/riverine input of particles with a low ^{210}Po / ^{210}Pb AR into the river-dominated shallow seas of the Arctic. The age of the particles and water masses as well as the importance of biogeochemical processes (e.g., respiration, remineralization) may also explain some of these observations, as there was a significant relationship between the total particulate activity ratio and AOU when both were measured in the North Atlantic (> 20° N) and Arctic oceans.

Over 80 % of the particulate radionuclide activity was on small particles, indicating that the scavenging of both radionuclides was driven by small particles. Therefore, we suggest considering the activities of ^{210}Po and ^{210}Pb from both small and large particles in order to study the water column

^{210}Po / ^{210}Pb disequilibria and quantify POC export along the GA01 transect. This has been addressed in a companion paper in this issue. We recommend that both small and large particles should be sampled for POC / ^{210}Po estimates for the application of the ^{210}Po / ^{210}Pb method in future studies of POC export.

Data availability. The total and particulate ^{210}Po and ^{210}Pb activity data from the GEOVIDE cruise can be found in the Supplement as Table S2.

The Supplement related to this article is available online at https://doi.org/10.5194/bg-15-5437-2018-supplement.

Competing interests. The authors declare that they have no conflict of interest.

Special issue statement. This article is part of the special issue "GEOVIDE, an international GEOTRACES study along the OVIDE section in the North Atlantic and in the Labrador Sea (GA01)". It is not associated with a conference.

Acknowledgements. Thank you to the chief scientists (Géraldine Sarthou and Pascale Lherminier) of the GEOVIDE cruise and the captain (Gilles Ferrand) and crew of the R/V *Pourquoi Pas?* for their support of this work. Many thanks to Pierre Branellec, Floriane Desprez de Gésincourt, Michel Hamon, Catherine Kermabon, Philippe Le Bot, Stéphane Leizour, Olivier Ménage, Fabien Pérault, and Emmanuel de Saint-Léger for their technical support during the GEOVIDE expedition, and to Catherine Schmechtig for the GEOVIDE database management. Phoebe Lam is also acknowledged for providing two modified McLane ISPs. Special thanks go to the members of the pump group, including Frédéric Planchon, Virginie Sanial, and Catherine Jeandel. The author would like to thank Clarisse Mariez, Stéphane Roig, Frédéric Planchon, and Hélène Planquette, who helped in providing particle composition data. We also would like to acknowledge the funding agencies: the French National Research Agency (ANR-13-BS06-0014, ANR-12-PDOC-0025-01), the French National Center for Scientific Research (CNRS-LEFE-CYBER), LabexMER (anr-10-LABX-19), and Ifremer. Funding was provided to Pere Masque by the Generalitat de Catalunya (grant 2017 SGR-1588). This work contributes to the ICTA "Unit of Excellence" (MinECo, MDM2015-0552). Gillian Stewart and Yi Tang were supported by NSF award #OCE 1237108. Maxi Castrillejo and Montserrat Roca-Marti were funded by an FPU PhD studentship (AP-2012-2901 and AP2010-2510, respectively) from the Ministerio de Educación, Cultura y Deporte of Spain. Maxi Castrillejo was also supported by the ETH Zurich Postdoctoral Fellowship Program (17-2 FEL-30), co-funded by the Marie Curie Actions for People COFUND program. Additional thanks go to Gary Hemming (Queens College) and Troy Rasbury (Stony Brook University) for laboratory assistance with the ICP-MS analyses. We also thank two anonymous reviewers for their constructive comments on how to improve the manuscript.

Edited by: Catherine Jeandel
Reviewed by: two anonymous referees

References

Amacher, J., Neuer, S., and Lomas, M.: DNA-based molecular fingerprinting of eukaryotic protists and cyanobacteria contributing to sinking particle flux at the Bermuda Atlantic time-series study, Deep-Sea Res. Pt. II, 93, 71–83, https://doi.org/10.1016/j.dsr2.2013.01.001, 2013.

Bacon, M. P.: ^{210}Pb and ^{210}Po results from F.S. "Meteor" cruise 32 in the North Atlantic, PANGAEA, https://doi.org/10.1594/PANGAEA.604014, 1977.

Bacon, M. P., Spencer, D. W., and Brewer, P. G.: ^{210}Pb / ^{226}Ra and ^{210}Po / ^{210}Pb disequilibria in seawater and suspended particulate matter, Earth Planet. Sc. Lett., 32, 277–296, https://doi.org/10.1016/0012-821X(76)90068-6, 1976.

Bacon, M. P., Brewer, P. G., Spencer, D. W., Murray, J. W., and Goddard, J.: Lead-210, polonium-210, manganese and iron in the Cariaco Trench, Deep-Sea Res. Pt. A, 27, 119–135, https://doi.org/10.1016/0198-0149(80)90091-6, 1980a.

Bacon, M. P., Spencer, D. W., and Brewer, P. G.: Lead-210 and Polonium-210 as Marine Geochemical Tracers: Review and Discussion of Results from the Labrador Sea, Natural radiation environment III, edited by: Gesell, T. F. and Lowder, W. M., 1, 473–501, 1980b.

Bacon, M. P., Belastock, R. A., Tecotzky, M., Turekian, K. K., and Spencer, D. W.: Lead-210 and polonium-210 in ocean water profiles of the continental shelf and slope south of New England, Cont. Shelf Res., 8, 841–853, https://doi.org/10.1016/0278-4343(88)90079-9, 1988.

Benetti, M., Reverdin, G., Lique, C., Yashayaev, I., Holliday, N. P., Tynan, E., Torres-Valdes, S., Lherminier, P., Tréguer, P., and Sarthou, G.: Composition of freshwater in the spring of 2014 on the southern Labrador shelf and slope, J. Geophys. Res.-Oceans, 122, 1102–1121, https://doi.org/10.1002/2016JC012244, 2017.

Bishop, J. K. B., Edmond, J. M., Ketten, D. R., Bacon, M. P., and Silker, W. B.: The chemistry, biology, and vertical flux of particulate matter from the upper 400 m of the equatorial Atlantic Ocean, Deep-Sea Res., 24, 511–548, https://doi.org/10.1016/0146-6291(78)90010-3, 1977.

BODC, Lowry, R. K., Machin, P., and Cramer, R. N.: Compilation of the results of EU-project BOFS, PANGAEA, https://doi.org/10.1594/PANGAEA.859221, 2016.

Boyer, T., Conkright, M. E., and Levitus, S.: Seasonal variability of dissolved oxygen, percent oxygen saturation, and apparent oxygen utilization in the Atlantic and Pacific Oceans, Deep-Sea Res. Pt. I, 46, 1593–1613, https://doi.org/10.1016/S0967-0637(99)00021-7, 1999.

Carmack, E., Barber, D., Christensen, J., Macdonald, R., Rudels, B., and Sakshaug, E.: Climate variability and physical forcing of the food webs and the carbon budget on panarctic shelves, Prog. Oceanogr., 71, 145–181, https://doi.org/10.1016/j.pocean.2006.10.005, 2006.

Ceballos-Romero, E., Le Moigne, F. A. C., Henson, S., Marsay, C. M., Sanders, R. J., García-Tenorio, R., and Villa-Alfageme, M.: Influence of bloom dynamics on Particle Export Efficiency in the North Atlantic: a comparative study of radioanalytical techniques and sediment traps, Mar. Chem., 186, 198–210, https://doi.org/10.1016/j.marchem.2016.10.001, 2016.

Clegg, S. L. and Whitfield, M.: A generalised model for the scavenging of trace metals in the open ocean: I. Particle cycling, Deep-Sea Res. Pt. A, 37, 809–832, https://doi.org/10.1016/0198-0149(90)90008-J, 1990.

Clegg, S. L. and Whitfield, M.: A generalied model for the scavenging of trace metals in the open ocean – II. Thorium scavenging, Deep-Sea Res. Pt. A, 38, 91–120, https://doi.org/10.1016/0198-0149(91)90056-L, 1991.

Cochran, J. K. and Masqué, P.: Short-lived U/Th Series Radionuclides in the Ocean: Tracers for Scavenging Rates, Export Fluxes and Particle Dynamics, Reviews in Mineralogy and Geochemistry, 52, 461–492, https://doi.org/10.2113/0520461, 2003.

Cochran, J. K., Bacon, M. P., Krishnaswami, S., and Turekian, K. K.: ^{210}Po and ^{210}Pb distributions in the central and eastern Indian Ocean, Earth Planet. Sc. Lett., 65, 433–452, https://doi.org/10.1016/0012-821X(83)90180-2, 1983.

Cooper, L.: Factors affecting the distribution of silicate in the North Atlantic Ocean and the formation of North Atlantic deep water, J. Mar. Biol. Assoc. UK, 30, 511–526, https://doi.org/10.1017/S0025315400012947, 1952.

Coppola, L., Prieur, L., Taupier-Letage, I., Estournel, C., Testor, P., Lefevre, D., Belamari, S., LeReste, S., and Taillandier, V.: Observation of oxygen ventilation into deep waters through targeted deployment of multiple Argo-O_2 floats in the northwestern Mediterranean Sea in 2013, J. Geophys. Res.-Oceans, 122, 6325–6341, https://doi.org/10.1002/2016JC012594, 2017.

Dugdale, R. C. and Goering, J. J.: uptake of new and regenrated forms of nitrogen in primary production, Limnol. Oceanogr., 12, 196–206, https://doi.org/10.4319/lo.1967.12.2.0196, 1967.

Duteil, O., Koeve, W., Oschlies, A., Bianchi, D., Galbraith, E., Kriest, I., and Matear, R.: A novel estimate of ocean oxygen utilisation points to a reduced rate of respiration in the ocean interior, Biogeosciences, 10, 7723–7738, https://doi.org/10.5194/bg-10-7723-2013, 2013.

Fleer, A. P. and Bacon, M. P.: Determination of ^{210}Pb and ^{210}Po in seawater and marine particulate matter, Nuclear Instruments and Methods in Physics Research, 223, 243–249, https://doi.org/10.1016/0167-5087(84)90655-0, 1984.

Flynn, W. W.: The determination of low levels of polonium-210 in environmental materials, Anal. Chim. Ac., 43, 221–227, https://doi.org/10.1016/S0003-2670(00)89210-7, 1968.

Fowler, S. W. and Knauer, G. A.: Role of large particles in the transport of elements and organic compounds through the oceanic water column, Prog. Oceanogr., 16, 147–194, https://doi.org/10.1016/0079-6611(86)90032-7, 1986.

Friedrich, J.: Polonium-210 and Lead-210 activities measured on 17 water bottle profiles and 50 surface water samples during POLARSTERN cruise ARK-XXII/2, PANGAEA, https://doi.org/10.1594/PANGAEA.763937, 2011.

Friedrich, J. and Rutgers van der Loeff, M. M.: A two-tracer (^{210}Po–^{234}Th) approach to distinguish organic carbon and biogenic silica export flux in the Antarctic Circumpolar Current, Deep-Sea Res. Pt. I, 49, 101–120, https://doi.org/10.1016/S0967-0637(01)00045-0, 2002.

Friedrich, J., Robert, M., and Stimac, I.: Polonium-210 and Lead-210 activities measured on 9 water bottle profiles during POLARSTERN cruise ANT-XXIV/3, PANGAEA, https://doi.org/10.1594/PANGAEA.763970, 2011.

García-Ibáñez, M. I., Pardo, P. C., Carracedo, L. I., Mercier, H., Lherminier, P., Ríos, A. F., and Pérez, F. F.: Structure, transports and transformations of the water masses in the Atlantic Subpolar Gyre, Prog. Oceanogr., 135, 18–36, https://doi.org/10.1016/j.pocean.2015.03.009, 2015.

GEOTRACES Planning Group: GEOTRACES Science Plan, Baltimore, Maryland, available at: http://www.geotraces.org/libraries/documents/Science_plan.pdf (last access: 7 September 2018), 2006.

Gourain, A., Planquette, H., Cheize, M., Menzel-Barraqueta, J. L., Boutorh, J., Shelley, R. U., Pereira-Contreira, L., Lemaitre, N., Lacan, F., Lherminier, P., and Sarthou, G.: Particualte trace metals along the GEOVIDE section, Biogeosciences Discuss., in preparation, 2018.

Hayes, C. T., Black, E. E., Andersen, R. A., Baskaran, M., Buesseler, K. O., Charette, M. A., Cheng, H., Cochran, J. K., Edwards, R. L., Fitzgerald, P., Lam, P. J., Lu, Y., Morris, S. O., Ohnemus, D. C., Pavia, F. J., Stewart, G., and Tang, Y.: Flux of particulate elements in the North Atlantic Ocean constrained by multiple radionuclides, Global Biogeochem. Cy., in review, 2018.

He, J., Yu, W., Lin, W., Men, W., and Chen, L.: Particulate organic carbon export fluxes on Chukchi Shelf, western Arctic Ocean, derived from 210Po/210Pb disequilibrium, Chin. J. Oceanol. Limn., 33, 741–747, https://doi.org/10.1007/s00343-015-3357-x, 2015.

Heyraud, M., Fowler, S. W., Beasley, T. M., and Cherry, R. D.: Polonium-210 in euphausiids: A detailed study, Mar. Biol., 34, 127–136, https://doi.org/10.1007/BF00390754, 1976.

Hong, G.-H., Park, S.-K., Baskaran, M., Kim, S.-H., Chung, C.-S., and Lee, S.-H.: Lead-210 and polonium-210 in the winter well-mixed turbid waters in the mouth of the Yellow Sea, Cont. Shelf Res., 19, 1049–1064, https://doi.org/10.1016/S0278-4343(99)00011-4, 1999.

Honjo, S., Spencer, D. W., and Gardner, W. D.: A sediment trap intercomparison experiment in the Panama Basin, 1979, Deep-Sea Res. Pt. A, 39, 333–358, https://doi.org/10.1016/0198-0149(92)90112-7, 1992.

Hu, W., Chen, M., Yang, W., Zhang, R., Qiu, Y., and Zheng, M.: Enhanced particle scavenging in deep water of the Aleutian Basin revealed by ^{210}Po- ^{210}Pb disequilibria, J. Geophys. Res.-Oceans, 119, 3235–3248, https://doi.org/10.1002/2014JC009819, 2014.

Ito, T., Follows, M. J., and Boyle, E. A.: Is AOU a good measure of respiration in the oceans?, Geophys. Res. Lett., 31, 1–4, https://doi.org/10.1029/2004GL020900, 2004.

Keeling, R. F., Stephens, B. B., Najjar, R. G., Doney, S. C., Archer, D., and Heimann, M.: Seasonal variations in the atmospheric O_2 / N_2 ratio in relation to the kinetics of air-sea gas exchange, Global Biogeochem. Cy., 12, 141–163, https://doi.org/10.1029/97GB02339, 1998.

Kim, G. and Church, T. M.: Seasonal biogeochemical fluxes of ^{234}Th and ^{210}Po in the Upper Sargasso Sea: Influence from atmospheric iron deposition, Global Biogeochem. Cy., 15, 651–661, https://doi.org/10.1029/2000GB001313, 2001.

Lam, P. J., Ohnemus, D. C., and Auro, M. E.: Size-fractionated major particle composition and concentrations from the US GEOTRACES North Atlantic Zonal Transect, Deep-Sea Res. Pt. II, 116, 303–320, https://doi.org/10.1016/j.dsr2.2014.11.020, 2015.

Lomas, M. W. and Moran, S. B.: Evidence for aggregation and export of cyanobacteria and nano-eukaryotes from the Sargasso Sea euphotic zone, Biogeosciences, 8, 203–216, https://doi.org/10.5194/bg-8-203-2011, 2011.

Masqué, P., Sanchez-Cabeza, J. A., Bruach, J. M., Palacios, E., and Canals, M.: Balance and residence times of ^{210}Pb and ^{210}Po in surface waters of the northwestern Mediterranean Sea, Cont. Shelf Res., 22, 2127–2146, https://doi.org/10.1016/s0278-4343(02)00074-2, 2002.

Menzel Barraqueta, J.-L., Schlosser, C., Planquette, H., Gourain, A., Cheize, M., Boutorh, J., Shelley, R., Pereira Contreira, L., Gledhill, M., Hopwood, M. J., Lherminier, P., Sarthou, G., and Achterberg, E. P.: Aluminium in the North Atlantic Ocean and the Labrador Sea (GEOTRACES GA01 section): roles of continental inputs and biogenic particle removal, Biogeosciences Discuss., https://doi.org/10.5194/bg-2018-39, in review, 2018.

Mercier, H., Lherminier, P., Sarafanov, A., Gaillard, F., Daniault, N., Desbruyeres, D., Falina, A., Ferron, B., Gourcuff, C., Huck, T., and Thierry, V.: Variability of the meridional overturning circulation at the Greenland–Portugal OVIDE section from 1993 to 2010, Prog. Oceanogr., 132, 250–261, https://doi.org/10.1016/j.pocean.2013.11.001, 2015.

Moore, R. M. and Smith, J. N.: Disequilibria between ^{226}Ra, ^{210}Pb and ^{210}Po in the Arctic Ocean and the implications for chemical modification of the Pacific water inflow, Earth Planet. Sc. Lett., 77, 285–292, https://doi.org/10.1007/978-94-011-3686-0_15, 1986.

Murray, J. W., Paul, B., Dunne, J. P., and Chapin, T.: ^{234}Th, ^{210}Pb, ^{210}Po and stable Pb in the central equatorial Pacific: Tracers for particle cycling, Deep-Sea Res. Pt. I, 52, 2109–2139, https://doi.org/10.1016/j.dsr.2005.06.016, 2005.

Nozaki, Y. and Tsunogai, S.: ^{226}Ra, ^{210}Pb and ^{210}Po disequilibria in the Western North Pacific, Earth Planet. Sc. Lett., 32, 313–321, https://doi.org/10.1016/0012-821X(76)90071-6, 1976.

Nozaki, Y., Dobashi, F., Kato, Y., and Yamamoto, Y.: Distribution of Ra isotopes and the ^{210}Pb and ^{210}Po balance in surface seawaters of the mid Northern Hemisphere, Deep-Sea Res. Pt. I, 45, 1263–1284, https://doi.org/10.1016/S0967-0637(98)00016-8, 1998.

Opsahl, S., Benner, R., and Amon, R. M. W.: Major flux of terrigenous dissolved organic matter through the Arctic Ocean, Limnol. Oceanogr., 44, 2017–2023, https://doi.org/10.4319/lo.1999.44.8.2017, 1999.

Peck, G. and Smith, J. D.: Uranium decay series radionuclides in the Western Equatorial Pacific Ocean and their use in estimating POC fluxes, edited by: Fernandez, J.-M. and Fichez, R., Paris, 459–469, 2002.

Puigcorbé, V., Benitez-Nelson, C. R., Masqué, P., Verdeny, E., White, A. E., Popp, B. N., Prahl, F. G., and Lam, P. J.: Small phytoplankton drive high summertime carbon and nutrient export in the Gulf of California and Eastern Tropical North Pacific, Global Biogeochem. Cy., 29, 1309–1332, https://doi.org/10.1002/2015GB005134, 2015.

Richardson, T. L. and Jackson, G. A.: Small Phytoplankton and Carbon Export from the Surface Ocean, Science, 315, 838–840, https://doi.org/10.1126/science.1133471, 2007.

Rigaud, S., Puigcorbé, V., Camara-Mor, P., Casacuberta, N., Roca-Martí, M., Garcia-Orellana, J., Benitez-Nelson, C. R., Masqué, P., and Church, T.: A methods assessment and recommendations for improving calculations and reducing uncertainties in the determination of ^{210}Po and ^{210}Pb activities in seawater, Limnol. Oceanogr.-Meth., 11, 561–571, https://doi.org/10.4319/lom.2013.11.561, 2013.

Rigaud, S., Stewart, G., Baskaran, M., Marsan, D., and Church, T.: ^{210}Po and ^{210}Pb distribution, dissolved-particulate exchange rates, and particulate export along the North Atlantic US GEOTRACES GA03 section, Deep-Sea Res. Pt. II, 116, 60–78, https://doi.org/10.1016/j.dsr2.2014.11.003, 2015.

Roca-Martí, M., Puigcorbé, V., Rutgers van der Loeff, M. M., Katlein, C., Fernández-Méndez, M., Peeken, I., and Masqué, P.: Carbon export fluxes and export efficiency in the central Arctic during the record sea-ice minimum in 2012: a joint ^{234}Th / ^{238}U and ^{210}Po / ^{210}Pb study, J. Geophys. Res.-Oceans, 121, 5030–5049, https://doi.org/10.1002/2016JC011816, 2016.

Roca-Martí, M., Puigcorbe, V., Friedrich, J., Rutgers van der Loeff, M. M., Rabe, B., Korhonen, M., Canara-Mor, P., Garcia-Orellana, J., and Masqué, P.: Distribution of ^{210}Pb and ^{210}Po in the Arctic water column during 2007 sea-ice minimun: particle export in the ice-covered basins, Deep-Sea Res. Pt. I, in review, 2018.

Sarin, M. M., Krishnaswami, S., Ramesh, R., and Somayajulu, B. L. K.: ^{238}U decay series nuclides in the northeastern Arabian Sea: Scavenging rates and cycling processes, Cont. Shelf Res., 14, 251–265, https://doi.org/10.1016/0278-4343(94)90015-9, 1994.

Sarin, M. M., Kim, G., and Church, T. M.: ^{210}Po and ^{210}Pb in the South-equatorial Atlantic, Deep-Sea Res. Pt. II, 46, 907–917, https://doi.org/10.1016/S0967-0645(99)00008-9, 1999.

Sarthou, G., Lherminier, P., Achterberg, E. P., Alonso-Pérez, F., Bucciarelli, E., Boutorh, J., Bouvier, V., Boyle, E. A., Branellec, P., Carracedo, L. I., Casacuberta, N., Castrillejo, M., Cheize, M., Contreira Pereira, L., Cossa, D., Daniault, N., De Saint-Léger, E., Dehairs, F., Deng, F., Desprez de Gésincourt, F., Devesa, J., Foliot, L., Fonseca-Batista, D., Gallinari, M., García-Ibáñez, M. I., Gourain, A., Grossteffan, E., Hamon, M., Heimbürger, L. E., Henderson, G. M., Jeandel, C., Kermabon, C., Lacan, F., Le Bot, P., Le Goff, M., Le Roy, E., Lefèbvre, A., Leizour, S., Lemaitre, N., Masqué, P., Ménage, O., Menzel Barraqueta, J.-L., Mercier, H., Perault, F., Pérez, F. F., Planquette, H. F., Planchon, F., Roukaerts, A., Sanial, V., Sauzède, R., Shelley, R. U., Stewart, G., Sutton, J. N., Tang, Y., Tisnérat-Laborde, N., Tonnard, M., Tréguer, P., van Beek, P., Zurbrick, C. M., and Zunino, P.: Introduction to the French GEOTRACES North Atlantic Transect (GA01): GEOVIDE cruise, Biogeosciences Discuss., https://doi.org/10.5194/bg-2018-312, in review, 2018.

Shelley, R. U., Roca-Martí, M., Castrillejo, M., Sanial, V., Masqué, P., Landing, W. M., van Beek, P., Planquette, H., and Sarthou, G.: Quantification of trace element atmospheric deposition fluxes to the Atlantic Ocean (> 40° N; GEOVIDE, GEOTRACES GA01) during spring 2014, Deep-Sea Res. Pt. I, 119, 34–49, https://doi.org/10.1016/j.dsr.2016.11.010, 2017.

Shimmield, G. B., Ritchie, G. D., and Fileman, T. W.: The impact of marginal ice zone processes on the distribution of ^{210}Pb, ^{210}Po and ^{234}Th and implications for new production in the Bellingshausen Sea, Antarctica, Deep-Sea Res. Pt. II, 42, 1313–1335, https://doi.org/10.1016/0967-0645(95)00071-W, 1995.

Smetacek, V., de Baar, H. J. W., Bathmann, U., Lochte, K., and Rutgers van der Loeff, M. M.: Export production by ^{234}Th, including ^{210}Po and ^{210}Pb measured on water bottle samples during POLARSTERN cruise ANT-X/6, PANGAEA, https://doi.org/10.1594/PANGAEA.89432, 1997.

Stanley, R. H. R., Doney, S. C., Jenkins, W. J., and Lott, III, D. E.: Apparent oxygen utilization rates calculated from tritium and helium-3 profiles at the Bermuda Atlantic Time-series Study site, Biogeosciences, 9, 1969–1983, https://doi.org/10.5194/bg-9-1969-2012, 2012.

Stewart, G., Cochran, J. K., Miquel, J. C., Masqué, P., Szlosek, J., Rodriguez y Baena, A. M., Fowler, S. W., Gasser, B., and Hirschberg, D. J.: Comparing POC export from ^{234}Th / ^{238}U and ^{210}Po / ^{210}Pb disequilibria with estimates from sediment traps in the northwest Mediterranean, Deep-Sea Res. Pt. I, 54, 1549–1570, https://doi.org/10.1016/j.dsr.2007.06.005, 2007.

Stewart, G. M., Fowler, S. W., and Fisher, N. S.: Chapter 8 The Bioaccumulation of U- and Th-Series Radionuclides in Marine Organisms, Radioactivity in the Environment, Elsevier, Vol. 13, 269–305, https://doi.org/10.1016/S1569-4860(07)00008-3, 2008.

Stewart, G. M., Bradley Moran, S., and Lomas, M. W.: Seasonal POC fluxes at BATS estimated from ^{210}Po deficits, Deep-Sea Res. Pt. I, 57, 113–124, https://doi.org/10.1016/j.dsr.2009.09.007, 2010.

Subha Anand, S., Rengarajan, R., Shenoy, D., Gauns, M., and Naqvi, S. W. A.: POC export fluxes in the Arabian Sea and the Bay of Bengal: A simultaneous ^{234}Th / ^{238}U and ^{210}Po / ^{210}Pb study, Mar. Chem., 198, 70–87, https://doi.org/10.1016/j.marchem.2017.11.005, 2017.

Tang, Y., Stewart, G., Lam, P. J., Rigaud, S., and Church, T.: The influence of particle concentration and composition on the fractionation of ^{210}Po and ^{210}Pb along the North Atlantic GEOTRACES transect GA03, Deep-Sea Res. Pt. I, 128, 42–54, https://doi.org/10.1016/j.dsr.2017.09.001, 2017.

Tang, Y., Lemaitre, N., Castrillejo, M., Roca-Martí, M., Masqué, P., and Stewart, G.: The export flux of particulate organic carbon derived from ^{210}Po / ^{210}Pb disequilibria along the North Atlantic GEOTRACES GA01 (GEOVIDE) transect, Biogeosciences Discuss., https://doi.org/10.5194/bg-2018-309, in review, 2018.

Tateda, Y., Carvalho, F. P., Fowler, S. W., and Miquel, J.-C.: Fractionation of ^{210}Po and ^{210}Pb in coastal waters of the NW Mediterranean continental margin, Cont. Shelf Res., 23, 295–316, https://doi.org/10.1016/s0278-4343(02)00167-x, 2003.

Tonnard, M., Planquette, H., Bowie, A. R., van der Merwe, P., Gallinari, M., Desprez de Gésincourt, F., Germain, Y., Gourain, A., Benetti, M., Reverdin, G., Tréguer, P., Boutorh, J., Cheize, M., Menzel Barraqueta, J.-L., Pereira-Contreira, L., Shelley, R., Lherminier, P., and Sarthou, G.: Dissolved iron in the North Atlantic Ocean and Labrador Sea along the GEOVIDE section (GEOTRACES section GA01), Biogeosciences Discuss., https://doi.org/10.5194/bg-2018-147, in review, 2018.

Towler, P.: Radionuclides measured on water bottle samples during FRANKLIN cruise FR05/92, PANGAEA, https://doi.org/10.1594/PANGAEA.104707, 2003.

Towler, P.: Radionuclides measured on water bottle samples during FRANKLIN cruise FR08/93, PANGAEA, https://doi.org/10.1594/PANGAEA.808075, 2013.

Verdeny, E., Masqué, P., Maiti, K., Garcia-Orellana, J., Bruach, J. M., Mahaffey, C., and Benitez-Nelson, C. R.: Particle export within cyclonic Hawaiian lee eddies derived from ^{210}Pb–^{210}Po disequilibrium, Deep-Sea Res. Pt. II, 55, 1461–1472, https://doi.org/10.1016/j.dsr2.2008.02.009, 2008.

Walsh, I. D. and Gardner, W. D.: A comparison of aggregate profiles with sediment trap fluxes, Deep-Sea Res. Pt. A, 39, 1817–1834, https://doi.org/10.1016/0198-0149(92)90001-A, 1992.

Wei, C., Lin, S., Wen, L., and Sheu, D. D. D.: Geochemical behavior of ^{210}Pb and ^{210}Po in the nearshore waters off western Taiwan, Mar. Pollut. Bull., 64, 214–220, https://doi.org/10.1016/j.marpolbul.2011.11.031, 2012.

Wei, C.-L., Yi, M.-C., Lin, S.-Y., Wen, L.-S., and Lee, W.-H.: Seasonal distributions and fluxes of ^{210}Pb and ^{210}Po in the northern South China Sea, Biogeosciences, 11, 6813–6826, https://doi.org/10.5194/bg-11-6813-2014, 2014.